Little Ice Age Cold Interval in West Antarctica: Evidence from Borehole Temperature at the West Antarctic Ice Sheet (WAIS) Divide.

Anais J. Orsi[1], Bruce D. Cornuelle[1] and Jeffrey P. Severinghaus[1].
[1]Scripps Institution of Oceanography, La Jolla, CA, USA

2012GL051260 - Supplementary material

1. Forward Model Description

The forward firn and ice model is based on the 1 dimensional heat and ice flow equation, discretized in an explicit finite difference scheme, following *Alley and Koci* [1990]:

$$\rho c_p \frac{\partial T}{\partial t} = \frac{\partial}{\partial z}\left(k \frac{\partial T}{\partial z}\right) - \rho c_p w \frac{\partial T}{\partial z} + Q \quad (1)$$

where ρ is the density of firn/ice, k the thermal conductivity, c_p the heat capacity, T the temperature, t the time, z the depth, w the downward velocity of the firn/ice, and Q the heat production term, taking into account ice deformation and firn compaction. WAIS Divide is near the ice flow divide, and the horizontal advection of mass and heat are both negligible.

a. Model Parameters

The density of ice, $\rho(z)$, is determined by a quadratic fit to measured bulk density data, following *Severinghaus et al.* [2010]. Data were collected on meter averages of cores coming from the WDC05A borehole by Todd Sowers [*Battle et al.,* 2011]. The density profile is considered to be in steady state.

The accumulation rate was taken as a constant 0.22 m_{ice}/yr [*Banta et al.,* 2008]. The year-to-year variability of the accumulation rate is on the order of 0.04 m/yr, and does not result in any significant difference in the temperature reconstruction. A detailed description of the influence of the accumulation rate is presented later in this document.

The vertical velocity of the firn or ice w is determined using a constant strain rate, following *Cuffey et al.,* [1994]**.** The heat capacity c_p, thermal conductivity k and heating term Q are all determined according to the classical equations [*Cuffey and Paterson*, 2010, Chapter 9]. They have a dependance on temperature, and are updated at each time step.

The depth of the firn/ice column is 3500 m, and no rock is modeled. We used a depth interval of 1 m for the first 500 m, and 25 m for the deeper section. The model is advanced by an explicit differentiation method, using 200 time steps per year for 2000 years.

b. Boundary Conditions

The model is initialized with a stationary temperature profile corresponding to a constant climate with a seasonal cycle, which is a simplified average of 3 years of weather station data from WAIS Divide and Byrd station (AMRC, SSEC, UW-Madison).

$$Tsea(t) = 10(cos(2\pi t) + 0.3cos(4\pi t)) \text{ (in K)} \quad (2)$$

The seasonal cycle does not change throughout the run, and the annual average temperature is the key evolving parameter.

Preliminary measurements of the 3400m deep borehole indicate melting at the bed [*Fudge et al.*, 2011]. We used a constant temperature and temperature gradient at the bed, consistent with those preliminary measurements. The influence of the bottom boundary condition is detailed in the next section.

2. Influence of the Initial Boundary Conditions

The initial temperature profile was set to a stationary profile with a realistic seasonal cycle. The real climate is not stationary, and long-term climate changes, such as the last ice age, may still have an imprint on the first 300 m of the ice sheet. It is not practical to extend the run time indefinitely. Thus the inversion scheme was run with a suite of initial temperature profiles to include the uncertainty associated with the unknown initial condition. Each optimization with variable initial conditions was

used to produce a series of 1000 solutions using Equation (6) of the main text. We used all 6000 solutions to derive the statistics presented in the main text.

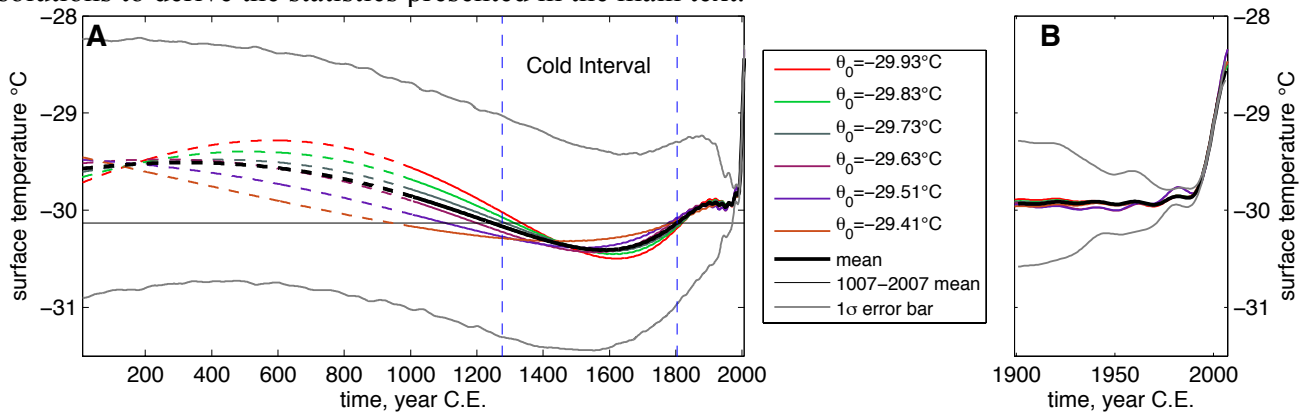

Figure S1: Sensitivity to the initial conditions. The colored line show the 2000-year reconstruction for a range of initial conditions. We used all of these runs as equally plausible solutions in our uncertainty estimation in the main text**.**

3. Influence of the Bottom Boundary Conditions

The bottom temperature and heat flux affect the steady state temperature profile, and the vertical velocity of the ice. In a thick ice sheet (WAIS is 3450m deep), and with a large accumulation rate (22cm/year), the advection of heat from the surface dominates the temperature distribution near the top of the ice sheet. It results that the steady state temperature profile is near isothermal for the first few hundred meters, and the boundary conditions at the bottom of the ice sheet are of limited importance.
We ran a series of sensitivity tests to quantify the effect of the bottom boundary on our reconstruction

c. Bottom Temperature

The bottom temperature was decreased from -4.68°C to -5.18°C. All other parameters, including the temperature history, were kept constant. This resulted in temperature differences smaller than 0.5mK in the top 300m of the ice sheet (Figure S2).

d. Bottom Temperature Gradient

The bottom temperature gradient reflects the amount of heat flux at the base of the ice. Preliminary measurements of the deep borehole show that there is a significant amount of heat flux at the bottom of WAIS. It is largely unknown how this flux may have changed in the past, but the fact that the ice is is young and undisturbed throughout most of the depth of the ice sheet suggests that the bottom of WAIS-Divide must have been melting throughout recent history [*Fudge et al.,* 2011]
We established the bottom temperature gradient to reflect the preliminary measurements of borehole temperature in the deep ice core hole. As a sensitivity test, we increased the bottom temperature gradient by 10%. There is no measurable change (less than 0.5mK) to the profile in the top 300m of the ice sheet (Figure S2).

e. Bottom Depth

Determining the depth of the ice sheet is challenging. It can be done by radar measurements, sonic imaging, or by extrapolating the temperature curve to the pressure melting point. For WAIS Divide, it is thought to be between 3440 and 3480m. We tested the influence on the geometry of our system by changing the depth of the domain from 3500m to 3400m. With all other parameters kept constant, it resulted in a temperature increase of 0.4mK at 300m, decreasing to 0 at the surface. This is insignificant in relation to the precision of our measurements.

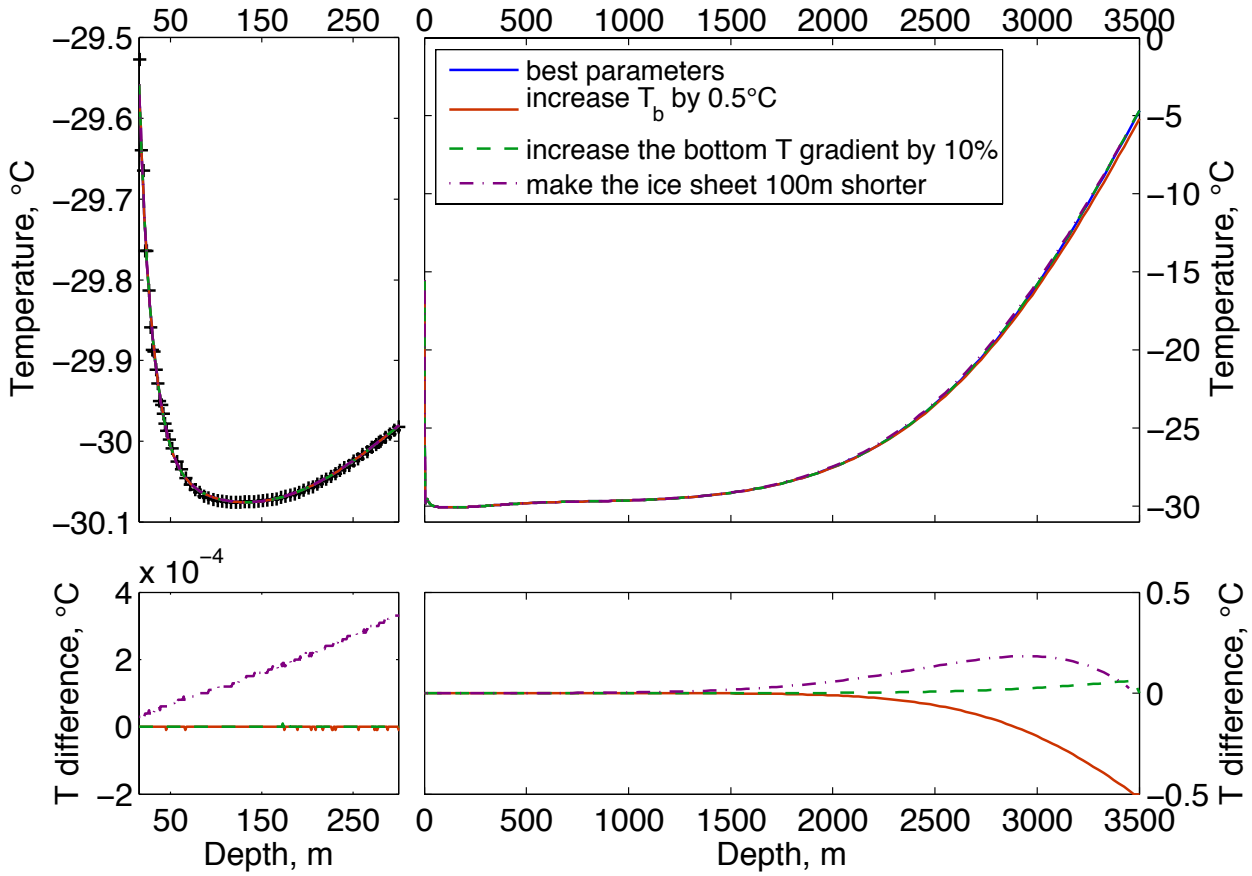

Figure S2: Sensitivity to the bottom boundary conditions. 3 tests are presented: 1) increase the bottom temperature by 0.5°C, 2) increase the bottom temperature gradient by 10%, which corresponds to a larger geothermal heat flux, 3) let the ice sheet thickness be 100m less. The top 2 panels show the temperature profile, the leftmost one being a zoom over the first 300m where we have data. The bottom panels show the change in the temperature profile obtained by each of these sensitivity tests. The top 1000m is not noticeably sensitive to changes in the bottom boundary conditions.

4. Influence of the Vertical Velocity Parameterization.

There are a few ways to express the vertical velocity profile. We followed *Alley et al.* [1990] and *Cuffey et al.* [1994] in using a vertical velocity profile corresponding to a constant strain rate. Another popular expression is derived from the analytical model of *Lliboutry et al.* [1979], as used by *Goujon et al.* [2003].

These two expressions produce marginally different vertical velocities in the top 300 m: the maximum difference is about 3.5 mm/yr (or 1.8%) at 300 m depth, and it increases to 18 mm/yr at 2800 m depth. It translates to 2 mK difference in the 300 m profile, and a 0.55°C difference at 2800 m. Getting a realistic parameterization of the vertical velocity is important at depth, but for the top of the ice sheet, our assumption does not affect the conclusions.

The uncertainty in the vertical velocity comes mainly from uncertainty in the accumulation rate: the vertical velocity is proportional to the accumulation rate, which is discussed in the next section.

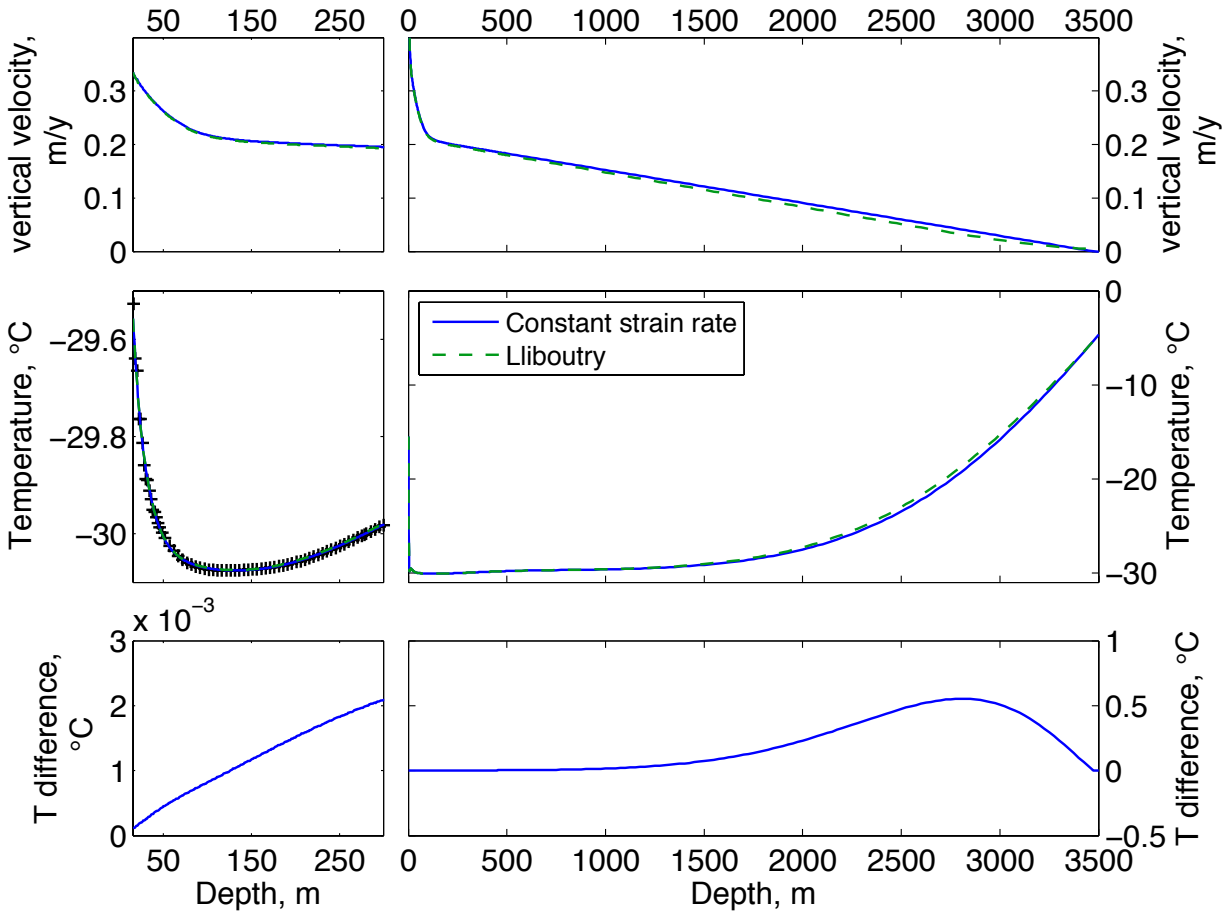

Figure S3: Comparison of the borehole temperature profile obtained from two different vertical velocity parameterizations: 1) constant strain rate [*Cuffey et al*, 1994], 2) Lliboutry [*Goujon* et al 2003]. The top panels show the vertical velocity, the middle panels the temperature profile, and the bottom panels the difference between both temperature profiles. On the left is a zoom over the 300m where we have data.

5. Influence of the Accumulation Rate

The model we use has a constant density profile, and only uses the accumulation rate in the calculation of the vertical velocity.

Banta et al [2008] have shown that the accumulation rate is on average 0.22 ± 0.04 m_{ice}/yr at WAIS Divide. We have run a sensitivity test including the variable layer-counting-derived accumulation rate for the last 230 years. It did not affect the temperature profile noticeably, mainly because the mean accumulation rate has not changed significantly. However, if we decrease the accumulation rate to 0.20 m/y, the same temperature anomaly will appear shallower in the ice, and the timing of the extrema will be affected. Decreasing the accumulation rate by 10% creates a temperature difference up to 10mK at 300m (third panel of Figure S4). It will have an effect on our reconstruction. We performed the same optimization for an accumulation rate of 0.20 m/y and found that the cold minimum was about 10% larger, and its timing offset by 39 years, which fits within the stated error in the main text.

Preliminary measurements of layer thickness in the deep ice core WDC06A indicate that the accumulation rate at WAIS Divide may not have changed by more than 10% over the last 2000 years (Joe McConnell, personal communication). This sensitivity test can be treated as an upper limit to the real variability.

A different model with a more sophisticated treatment of the downward motion of the ice could produce a more detailed result.

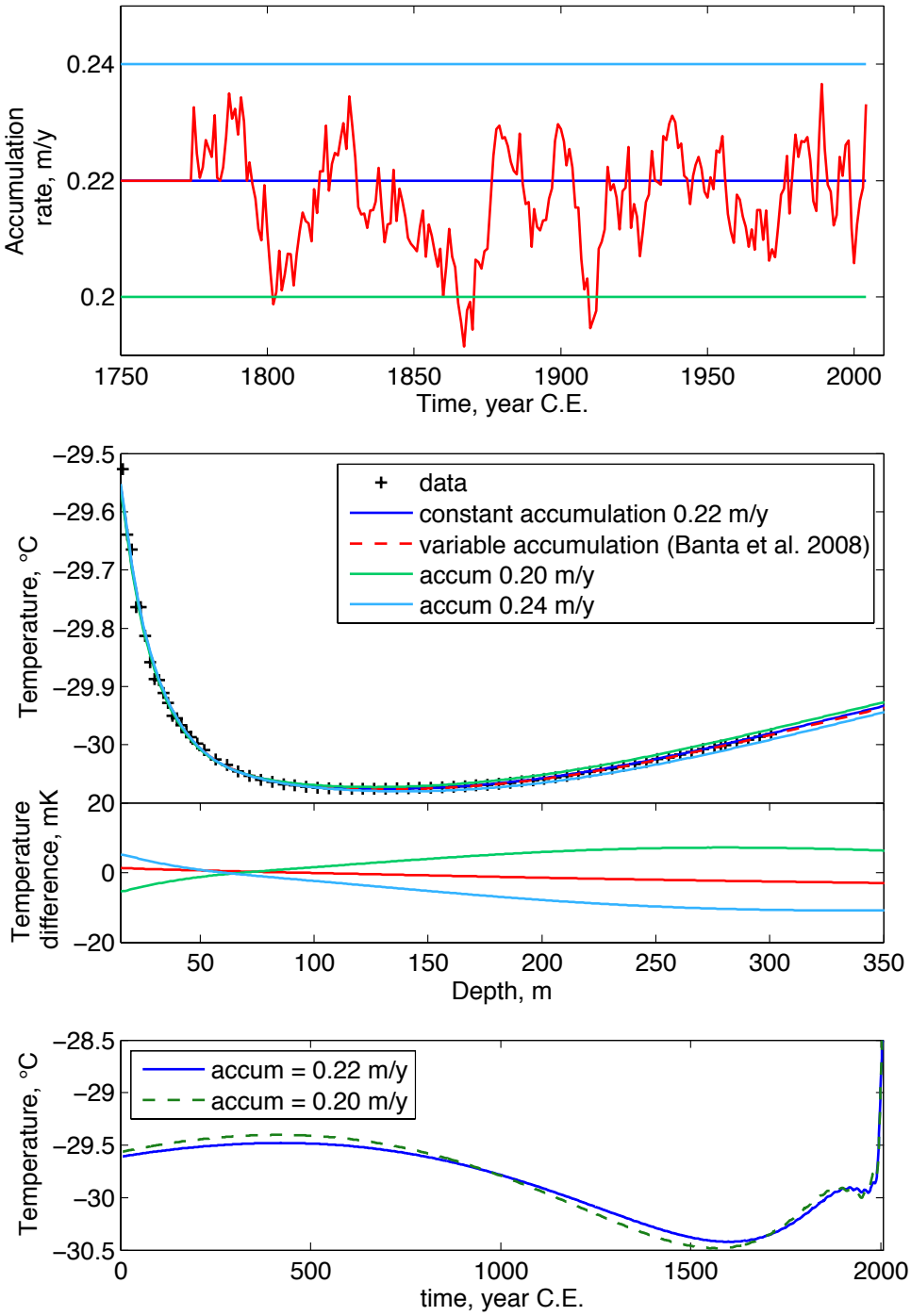

Figure S4: Influence of the accumulation rate. Four scenarios are compared: 1) constant accumulation rate at 0.22 m/yr, 2) variable accumulation rate for the last 230 years according to *Banta et al.,* [2008], 3) constant accumulation rate at 0.20 m/y, 4) constant accumulation rate at 0.24 m/y. The top panels show the accumulation rate history that served as an input. The second panel shows the temperature profile for the first 350 m, with all other inputs unchanged. The third panel shows the difference between scenarios 2, 3, and 4, and scenario 1. The bottom panel shows the reconstruction based on an accumulation rate of 0.20 m/y, with an improved fit to the data, and the initial temperature reconstruction using 0.22 m/y. The reduction in the accumulation rate requires an increase in the amplitude of climate changes, and a shift of the extrema towards earlier times.

6. Influence of the Thermal Conductivity of the Ice.

The thermal conductivity of the ice is difficult to parameterize because it depends not only on density, but also on the type of packing of the snow grains. We used the Schwerdtfeger formula [*Cuffey and Patterson*, 2010, Chapter 9], which depends on both temperature and density of the snow. It usually gives an upper estimate of the thermal diffusivity of snow. We decreased the thermal conductivity by 10%, and ran the optimization of the temperature again. It resulted in a shift of the timing of the main temperature minimum by 58 years (earlier), but no change in the amplitude of the signal (Figure S5). We observed a similar shift when decreasing the initial temperature by 0.1°C.

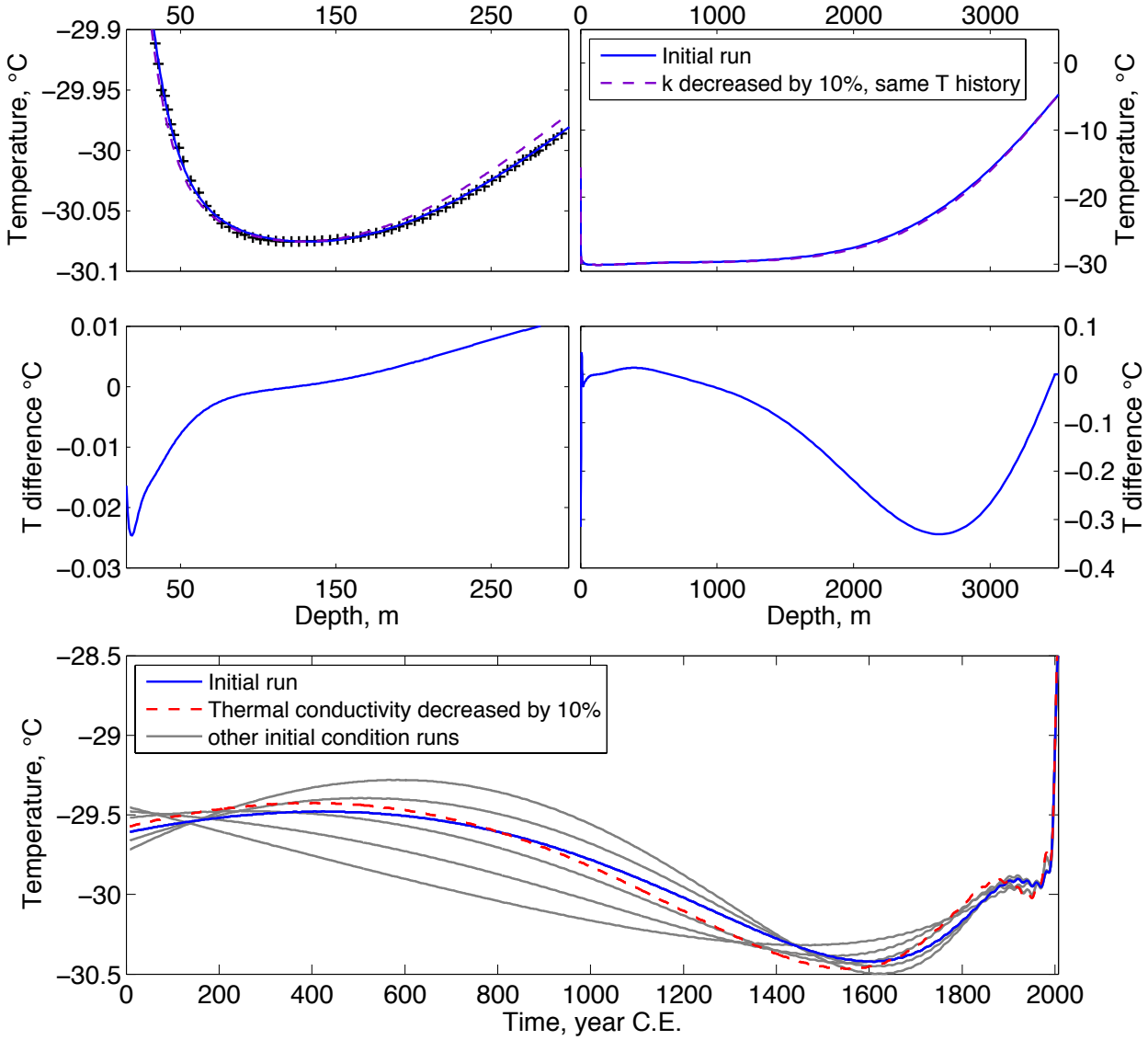

Figure S5: Sensitivity to a 10% decrease in the thermal conductivity. The top panels show the temperature profiles, with the initial run, and the 10% lower *k* run, using all other parameters equal. On the left is a zoom over the 300m where we have data (black + signs). The middle panels show the difference between these two profiles. The bottom panel shows the initial temperature reconstruction used as a boundary condition in blue, the optimal temperature reconstruction for a 10% lower thermal conductivity in dashed red, and optimal solutions for other initial conditions as presented in Figure 3 of the main text, to give an idea of the uncertainty in the reconstruction. Lowering the thermal conductivity creates a shift in time, but no change in the amplitude of the extrema.

7. Influence of the Basis Functions Used in the Inversion.

a. Influence of the Prior Covariance of the Model Parameters

The shape of the solution is determined in part by the choice of the covariance matrix of the model parameters (denoted by **P** in the main text). Our assumptions about what constitutes an acceptable solution are manifested in the choice of the matrix **P**. We made three assumptions:

1) The variability of the climate should not be more than order 0.5°C. This value was chosen in the range of published changes in climate. *Dahl Jensen et al.* [1999] found a variability on the order of 0.3°C using a Monte Carlo inversion of the Law Dome (Antarctica) borehole temperature profile.
2) The low frequencies are favored over the high frequencies: we will favor a long-term climate change over a shorter-lived event of larger amplitude.
3) The prior spectrum is stationary: Every point in time is given the same decorrelation timescale.

There are several ways to weigh the low frequencies. *Shen et al* [1992] discussed a range of choices for the matrix P.

We used the standard inverse-square frequency f^2 spectrum, which translates into choosing $P_{i,i} = \sigma_x^2 \frac{f(i)^{-2}}{\sum_i f(i)^{-2}}$ with $f(i)$ the frequency of the sin/cos used in the basis functions, and σ_x=0.5°C the a-priori root mean square error of the model parameters. This reconstruction is represented by the green curve in Figure S6.

As a sensitivity test, we also used $P_{i,i} = \sigma_x^2 \frac{(f(i)+f_o)^{-2}}{\sum_i (f(i)+f_o)^{-2}}$ with an offset f_o=1/270 yr^{-1} (red curve in Figure S6). This means that the prior spectrum is a little less red, and the higher frequencies have a slightly larger variance. If we let f_o be too large, the amplitudes of the lowest frequencies become larger than expected, which violates our assumptions. This solution allowed a higher frequency structure, which is reflected in the reconstruction by the absence of a bump circa 400 C.E. in the red curve compared to the blue, and the temperature extrema being slightly closer to the present.

We also tried a Gaussian spectrum $P_{i,i} = \sigma_x^2 \exp\left(-\frac{f(i)}{f_o}\right)$ with an e-folding scale f_o=1/67 yr^{-1} (blue curve in Figure S6). A Gaussian spectrum damps out the high frequencies faster than f^{-2}. In our data, we need enough high frequencies to fit the most recent times. The Gaussian spectrum did not perform as well as the f^2 spectrum.

Each spectrum can be converted into a covariance by computing BPB^T, which shows the timescales allowed. Figure S6 shows the best temperature history found with each one of these prior covariance matrices, along with the misfit with the data, and the prior covariance matrix plotted in the time domain. As the spectrum gets whiter (favoring high frequencies), the covariance between different times diminishes, which will increase our error bars, because we are not able to resolve fast changes in the climate.

It should be noted that the prior covariance has a limited effect on the least square optimum, but is a dominant component of the posterior error estimate $\hat{P}$. In other words, the prior spectrum defines our error bars: by choosing a relatively short decorrelation timescale, we allow the temperature to change fast, which will increase the error bars in our reconstruction. We considered that the short decorrelation timescale needed to resolve the recent warming should apply to the whole 2000-year reconstruction. Had we chosen a much larger correlation in the more distant past, the error bars would have been much smaller. The choice we made produces a very conservative error estimation of the Seventeenth century minimum.

b. Influence of the Signal to Noise Ratio:

If the signal to noise ratio is increased, the fit to the data increases, and the amplitude of the extrema also increases. We choose a signal to noise ratio consistent with previous studies, taking care to avoid it being too high and creating spurious extrema.

c. Influence of the Basis Function

We chose to use Fourier Series for a basis functions in order to keep the same baseline assumption of no change with the climate, and no change in the variability in the climate over all time periods. Choosing a stationary prior helps reduce the tendency to over-emphasize the abnormality of the recent warming.

As an alternative to Fourier Series, we used piecewise linear functions to describe the space of temperature history, with a time correlation decreasing towards the present (Purple curve in Figure S6). The matrix **P** is a little different, which induces a different optimal solution, but it shares the same basic characteristics with the other solutions: a temperature minimum between 1400 and 1800 C.E., and a large increase in temperature over the last 50 years. The variations in the timing of the large minimum reflect the uncertainty associated with this timing.

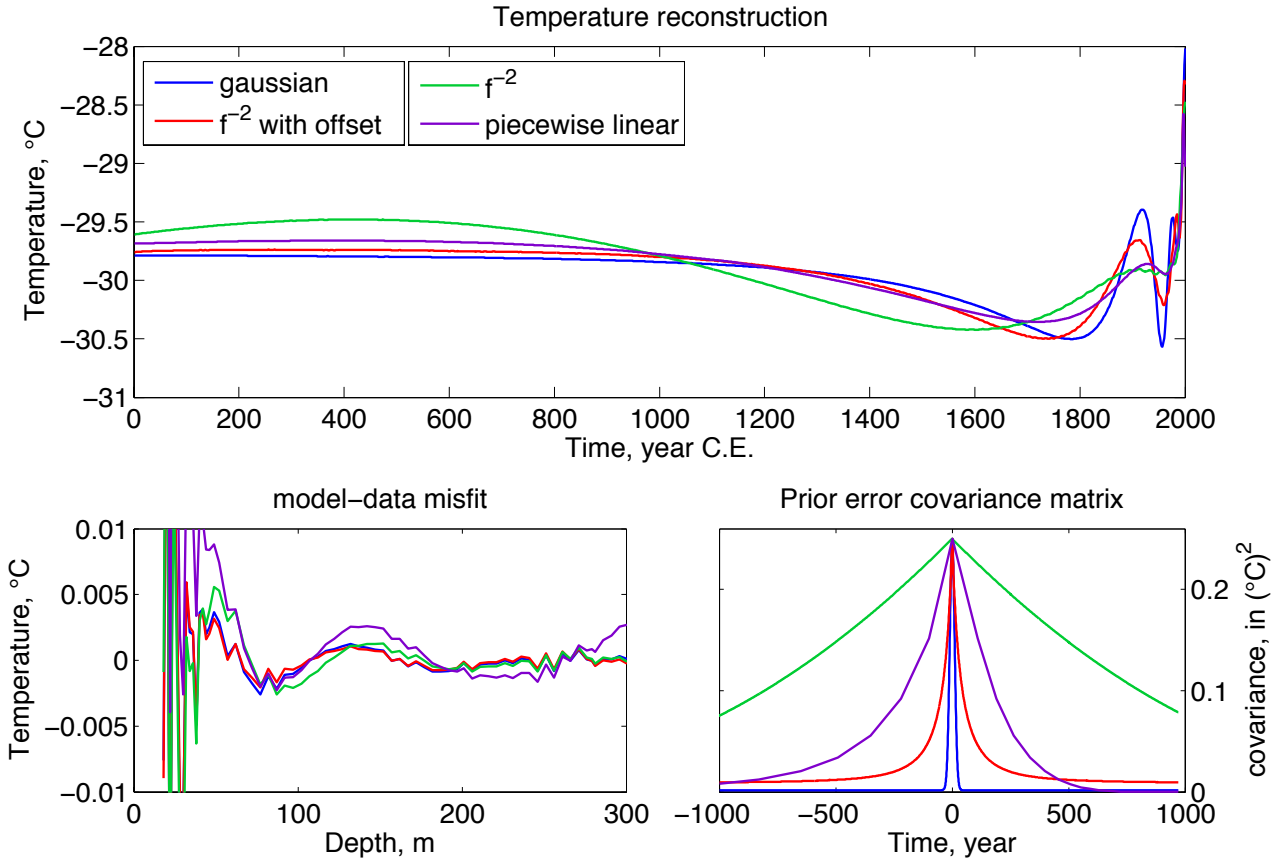

Figure S6: Influence of the prior covariance and basis functions used in the linearization. The blue line shows the reconstruction using Fourier series, with a Gaussian spectrum. The red line shows the reconstruction using Fourier series, with a quadratic spectrum with an offset**.** The green line shows the reconstruction for a Fourier decomposition, with simple quadratic spectrum. The purple line shows the optimal solution found using a piecewise linear decomposition with the same signal to noise ratio of 250.

The bottom left panel shows the misfit between the temperature profile corresponding to each of these temperature histories, and the data. Note that they do not all fit the data in the same way, but they are all within the stated error.

The bottom right panel shows the prior covariance matrix of the modeled temperature as a function of time difference with the reference time at the center. The covariance is stationary, meaning the same for all reference times. The narrower the covariance, the more weight is given to high frequencies, which is reflected in the reconstruction (top): shorter period are supplanted by longer periods.

8. Uncertainty in the Measurements

Uncertainties in the measurements are of two types: systematic biases, which affect the accuracy of the absolute value of the temperature measurement, and random noise, which may affect each data point separately. With respect to the borehole temperature problem, we are not as concerned by biases affecting the whole data set uniformly, as we are about errors that can be wrongly interpreted as climate signals.

In the following section, we have separated out the uniform biases, and the noise, which affects the reproducibility of one measurement to the next, and which is of a higher concern. The dominant source of uncertainty is the calibration of the thermistor, which has both types of error, and is treated first.

a. Uncertainty in the Calibration

The thermistor was measured against a secondary standard platinum resistance thermometer (Burns Engineering 12001, with a Hart 1502 readout), in a chilled ethanol bath between -40°C and -20°C. The PRT has an expanded uncertainty of 0.006°C, but we consider that the long-term drift of the probe from the time of NIST calibration may be as much as 0.1°C (worst case scenario). The repeat uncertainty of this probe in the range -38 to 0°C is typically 0.003°C and can be as much as 0.010°C (manufacturer specifications).

The calibration was done following the Steinhart-Hart equation:

$$1/T = a_1 + a_2 \times ln(R) + a_3 \times ln(R)^3$$

with T the temperature in K, R the resistance in kΩ, and the coefficients

$a_1 = 3.00805e^{-3} \pm 3.6e^{-10}$, $a_2 = 3.0665027e^{-04} \pm 5.8e^{-11}$ and $a_3 = -5.7055528e^{-07} \pm 3.14e^{-14}$

The propagation of error in the calibration, supposing that the Steinhart-Hart equation is a near perfect determinant of the temperature behavior of the probe, produces an uncertainty of 2.3 mK in the range of our borehole measurements: -29.4 to -30.8°C.

For this set of measurements, we consider the accuracy of our calibration to be 0.1°C, and its precision to be 2.3 mK.

b. Systematic Biases

In addition to systematic bias in the calibration of the probe, several artifacts can bias the measurements.

The **self heating** of the probe can create a positive bias, uh. We estimated the self heating for a heating rate $hr = 1$ mW/°C in air, a source current of $I = 10$ μA, and resistance of $R = 40$ kΩ. It is $uh = I^2 \times R/hr = (1e^{-5})^2 \times 4e^5/1e^{-3} = 0.04$°C.

We always used the same source current, but the resistance varied by 1.4 kΩ, which includes a potential bias of 1.4 mK over the range of measurements. The self heating was limited by only switching the system ON for a short period of time: in between measurements, the multimeter was turned off, and the probe was allowed to equilibrate with the ambient temperature. The procedure was replicated exactly for every sample, to ensure that the same amount of self heating was introduced into the measurements. Thus self heating bias was likely to be uniform across the data set.

The leads may have a certain amount of **current leakage**. The current leakage is estimated to create a bias $ul = 1/a*R/(R+Rl) = 0.6$mK, with $a = 0.0611$ the probe temperature coefficient, R the thermistor resistance ($R \approx 40$ kΩ), and Rl the critical leakage path resistance ($Rl \geq 1$GΩ). We used a 1000ft spool of wire, with 4 wires to limit the uncertainty in the lead wire resistance. We also inspected the wire for any breaks in the shielding, and found that it was in perfect condition.

Both the self heating and current leakage effects are accounted for in the calibration.

Hysteresis effects were minimized by measuring the temperature after a 20 min equilibration time, and by measuring the temperature both going upwards and downwards. There was no significant difference between upward and downward measurements: the mean difference was 0.95 mK, which is within the

stated uncertainty. We used the scanning function of our precision multimeter to verify that the temperature had reached a plateau before starting the measurement integration at each depth.

When measuring temperature in an air borehole, we need to consider the possibility of **cold air sinking** to the bottom of the borehole in winter and biasing our measurements. We measured the temperature during 2 summer Antarctic seasons, and found that the mean difference between the profiles taken in 2008 versus 2009 was 1.6 mK below 100 m (2009 was colder), which is within the stated uncertainty. Therefore, we do not anticipate any cold bias from sinking air.
Likewise, we do not expect a warm bias due to **thermal disturbance during drilling**, which occurred in January 2005, because this disturbance should have decreased with time.
Near the surface, solar radiation and **wind pumping** can have a leading effect on the temperature of the first 10 to 20 m. For that reason, we did not use the first 15 m of the temperature profile in our inversion.

c. Random Noise

The **temperature resolution** of a Kelvin circuit can be calculated as $ur = \Delta R/(a*R) = 0.1/(0.0611*40000) = 4e^{-5}$ K, with ΔR=100 mΩ the resolution of the readout, a = 0.0611 the probe temperature coefficient, and R the thermistor resistance (R≈40 kΩ). Clearly, this is not a considerable source of uncertainty in our measurement.
The most important source of random noise are the **electrostatic charges** building up near the instrument: On the ice sheet, there is no ground, and the wind can cause a large amount of electrostatic charge to build up on the walls of the nylon tent or on dangling cables. We limited the static buildup by keeping all other electric charges (like the snowmobile) away from the measurement tent, limiting the movements of the electrical wire, and limiting movements of the operator while measuring. We also used 12 V batteries with an inverter to power the multimeter, in order to avoid static buildup from a DC generator. It is difficult to establish how much noise may have been caused by electric charge buildup, but it is reasonable to expect that repeat measurements with several days in between, and from year to year should average out potential errors.
High frequency noise was limited by integrating the resistance reading over 5 minutes. Other random processes were taken into account by taking repeat measurements over several days.
The standard deviation of repeat measurements in the field was 1.8 mK below 50 m. This number integrates all sources of random noise, and represents the overall reproducibility of our measurements. It is better than the uncertainty in the calibration (2.3 mK), highlighting the fact that the calibration is the dominant source of uncertainty.

References:

Alley, R. B., and B. R. Koci, Recent warming in central Greenland?, *Annals of Glaciology*, *14*, 6–8, 1990.

Banta, J., J. McConnell, M. Frey, R. Bales, and K. Taylor, Spatial and temporal variability in snow accumulation at the West Antarctic Ice Sheet Divide over recent centuries, *Journal of Geophysical Research*, *113*(D23), 2008.

Battle, M. O., J. P. Severinghaus, E. D. Sofen, D. Plotkin, A. J. Orsi, M. Aydin, S. A. Montzka, T. Sowers, and P. P. Tans, Controls on the movement and composition of firn air at the West Antarctic Ice Sheet Divide, *Atmospheric Chemistry and Physics*, *11*(21), 11,007–11,021, 2011.

Cuffey, K., and W. Paterson, *The physics of glaciers*, Academic Press, 2010.

Cuffey, K., R. Alley, P. Grootes, J. Bolzan, and S. Anandakrishnan, Calibration of the delta super (18) o isotopic paleothermometer for central greenland, using borehole temperatures, *Journal of Glaciology*, *40*(135), 341–349, 1994.

Dahl-Jensen, D., V. I. Morgan, and A. Elcheikh, Monte carlo inverse modelling of the Law Dome (Antarctica) temperature profile, *Annals of Glaciology 145-150(6)*, *29*(1), 145–150(6), 1999.

Fudge, T., et al., WDC06A-5 An Annualy resolved timescale to 40ka and a case for high basal melt rate., in *WAIS Divide Science Meeting*, 2011.

Goujon, C., J.-M. Barnola, and C. Ritz (2003), Modeling the densification of polar firn including heat diffusion: Application to close-off characteristics and gas isotopic fractionation for Antarctica and Greenland sites, *J. Geophys. Res.,* 108(D24), 4792, doi:10.1029/2002JD003319.

Lliboutry, L., A critical review of analytical approximate solutions for steady state velocities and temperatures in cold ice-sheets, *Z. Gletscherkd. Glazialgeol*., 15(2), 135–148, 1979.

Severinghaus, J. P., et al., Deep air convection in the firn at a zero-accumulation site, central Antarctica, *Earth and Planetary Science Letters*, *293*(3-4), 359 – 367, DOI: 10.1016/j.epsl.2010.03.003, 2010.

Shen, P., K. Wang, H. Beltrami, and J. Mareschal, A comparative study of inverse methods for estimating climatic history from borehole temperature data, *Palaeogeography, Palaeoclimatology, Palaeoecology*, *98*(2-4), 113–127, 1992.